ACS APPLIED MATERIALS & INTERFACES

Research Article

www.acsami.org

Surface Plasmon Resonance Enhanced Polymer Solar Cells by Thermally Evaporating Au into Buffer Layer

Mengnan Yao,[†] Xu Jia,[†] Yan Liu,[‡] Wenbin Guo,[†] Liang Shen,*[,†] and Shengping Ruan[†]

[†]State Key Laboratory on Integrated Optoelectronics, College of Electronic Science and Engineering, Jilin University, 2699 Qianjin Street, Changchun 130012, People's Republic of China

[‡]Key Laboratory of Bionic Engineering (Ministry of Education), Jilin University, Changchun 130022, People's Republic of China

ABSTRACT: Generally, the surface plasmon resonance (SPR) effect of metal nanoparticles is widely applied on polymer solar cells (PSCs) to improve device performance by doping method into solution. Herein, a diameter-controlled thermally evaporation method was used to realize Au nanoparticles (Au NPs) doping into WO_3 anode buffer layer in inverted PSCs. The surface energy differences between Au and WO_3 inevitably lead to Au growing up through the process from nucleation, isolated island, aggregation of metal islands to continuous films along with the process of evaporation. The atom force microscopy (AFM) images indicate that critical thickness of Au film formation is 8 nm, which is in accordance with current density−voltage (J−V) and incident photon-to-electron conversion efficiency (IPCE) measurement results of optimal device performance. The power conversion efficiency (PCE) with 8 nm Au is dramatically improved from 4.67 ± 0.13% to 6.63 ± 0.17% compared to the one without Au. Moreover, the optical absorption enhancement is demonstrated by steady state photoluminescence (PL), which agrees well with transmission spectrum. The optical and electrical improvement all suggest that thermal evaporation is the appropriate method to further enhance device performance.

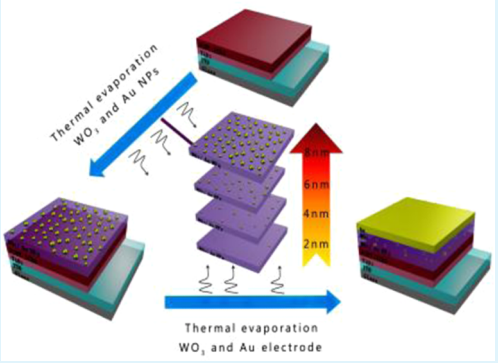

KEYWORDS: *surface plasmon resonance, transmittance, photoluminescence, thermally evaporation, buffer layer, polymer solar cells*

1. INTRODUCTION

Polymer solar cells (PSCs) offer a compelling option for further photovoltaic application due to their unique properties, such as lightweight, low-production-cost, mechanical flexibility, solution processability, and potential for large-area manufacture.[1−4] In the past few years, research on PSCs has deeply examined almost all aspects, including materials synthesis of electron donors and acceptors, interface modification, nanoparticles doping, light trapping method, tandem structure, and so on, which led to a significant power conversion efficiency (PCE) enhancement to more than 10%.[5−11] However, the still relatively low PCE, compared with inorganic solar cells, limits its further application. Seen from the fundamental working mechanism of PSCs, the external quantum efficiency (EQE) is determined by multiplication by internal quantum efficiency and absorption efficiency.[12,13] Despite the high absorption coefficients (>10^5 cm^{-1}) of many polymer materials, it is still difficult to absorb sufficient light for utilization in PSCs due to the relatively large bandgap compared to the one of silicon materials. However, comparatively small charge carrier mobilities (almost less than 10^{-3} $cm^2/(V\ s)$) and short exciton diffusion lengths on the order of magnitude of ∼10 nm limits the increasing thickness of the active absorber layer.[14−16] Therefore, the fundamental trade-off between efficient light absorption (which requires a thick active layer) and efficient photogenerated carriers collection (which requires a thin active layer) is a major barrier against further improvement of PSCs, which results in a case where increasing the light absorption of the active layer in a limited thickness becomes a challenge.[17−21] Recently, a variety of light-trapping techniques have been widely investigated looking into this situation, definitely including microcavity structure,[22−26] photonic crystals,[27−30] and plasmonic nanostructures.[31−35] However, the microcavity effect usually enhances the light absorption more remarkably in a device with a thinner active layer, and thus is not in good agreement with our initial intent to take full advantage of incident light. Moreover, a one-dimensional photonic crystal generally acts as a wavelength-dependent filter with a narrow range in specific spectrum, and other photonic crystals with two or three dimensions have to deal with the active layer with special techniques.

Among the proposed light trapping methods, in particular, plasmonic nanostructures based on advantageous optical properties have attracted considerable attention due to their unique tunable optical resonance features and near-field concentrations for enhancing light absorption by means of increasing the photocurrents of PSCs.[36] The metallic nanoparticles (NPs), such as Ag, Pt, Cu, and Au embedded in a

Received: June 27, 2015
Accepted: July 31, 2015
Published: July 31, 2015

DOI: 10.1021/acsami.5b05747
ACS Appl. Mater. Interfaces 2015, 7, 18866−18871

dielectric matrix, can strongly interact with light at their dipole surface plasmon frequency due to the excitation of a collective electron motion inside the NPs.[37−42] The surface confines the conduction electrons inside the NPs and sets up an effective restoring force, leading to resonant behavior at the dipole surface plasmon frequency, namely surface plasmon resonance (SPR). In addition, the incident photons can be scattered over a longer propagation path in the active layer by metallic nanostructures. The factors such as morphology, size, concentration, dielectric functions of the metal materials, and the dielectric surrounding environment of the metallic NPs can also influence the SPR effect. Therefore, the SPR effect has the potential to be utilized in PSCs to help to convert solar energy into electrical supply, resulting in a higher efficiency.[43−46] There have been lots of reports about PCE enhancement of PSCs by employing SPR within the devices, which mainly focused on metallic NPs with different sizes doped into the active layer. However, the synthesis process of metallic NPs is relatively complex, and grain diameter is different to control.[47,48] Herein, we present a simple thermally evaporated technique to introduce Au NPs into the anode buffer layer of inverted PSCs to enhance light absorption by SPR. Compared to solution-processable Au NPs to trigger the SPR, the differences of the surface energy between Au NPs and WO_3 lead to a gradual increase in the diameter of Au NPs instead of forming a gold film, and the grain diameter can be easily modulated by the evaporating thickness. We determine that the PSCs incorporating 8 nm-thick Au NPs exhibit a dramatically improved PCE from 4.67 ± 0.13% to 6.63 ± 0.17% compared to the one without Au. Moreover, steady state PL provides direct evidence that the SPR of Au NPs induces light absorption enhancement, which also agrees well with the transmission spectrum. Furthermore, the complex impedance also reveals that 8 nm-thick Au can decrease the device resistance effectively. The optical and electrical improvements all suggest that thermal evaporation is an appropriate method to further enhance device performance.

2. EXPERIMENTAL SECTION

The PSCs investigated in this paper have a structure of ITO/TiO_2/poly(3-hexylthiophene)/Indene-C_{60} bisadduct (P3HT:ICBA)/ WO_3/Au NPs/WO_3/Au, which is shown schematically in Figure 1. In the

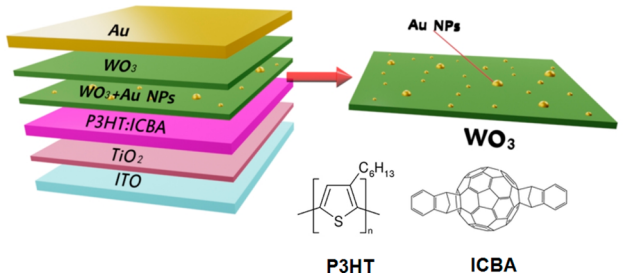

Figure 1. Device structure of the inverted PSCs by thermally evaporating Au NPs into WO_3 layer, with the chemical structure of P3HT and ICBA.

fabrication, ITO-coated glass substrates (a sheet resistance of 15 Ω/sq) were precleaned by ultrasonic treatment in detergent, deionized water, acetone and isopropy alcohol sequentially, and blown-dry with pure nitrogen flow. Anatase TiO_2 thin films were prepared as described in our previous papers to act as the electron transport layer (ETL).[49] P3HT (Lumtec Corp, used as received) blending with ICBA (Lumtec Corp, used as received) in 1:1 weight ratio was dissolved in 1,2-Dichlorobenzene. The blend was stirred for 72 h in glovebox filled with argon. Then, the P3HT/ICBA active layer was prepared by spin coating on top of TiO_2 film, and the thickness is about 200 nm, determined by Step Profiler measurement. Finally, the samples were evaporated with 5 nm WO_3, x nm Au (x = 2, 4, 6, 8, 10), 5 nm WO_3 and 100 nm Au in sequence under a high vacuum (5×10^{-4} Pa) without disrupting the vacuum. The deposition rate was about 0.1 nm/s, which was monitored by a quartz-oscillating thickness monitor (ULVAC, CRTM-9000). As we all know, WO_3 is an effective anode buffer layer in PSCs, and the optimal thickness is 10 nm reported by our pervious paper.[50] The active area of the device was 0.064 cm^2. The light intensity was measured with a photometer (International Light, IL1400), which was corrected by a standard silicon solar cells. UV-1700 was used to characterize the absorption ability of Au layer in the wavelength range from 300 to 1000 nm. The IPCE spectra for the cells were measured with Crowntech QTest Station 1000AD. AFM measurements in air were performed using a Solver Scanning Probe Microscope in tapping mode. Impedance spectroscopy, which measures the dielectric properties of a material and interface as the function of frequency, was measured by an impedance analyzer (Wayne Kerr Electronics 6520B) with a bias of 1 V in the frequency range of 20 Hz to 2 MHz.

3. EXPERIMENTAL AND SIMULATION RESULTS AND DISCUSSION

Figure 2a displays the representative $J-V$ characteristics, recording the performance of PSCs prepared using WO_3 buffer

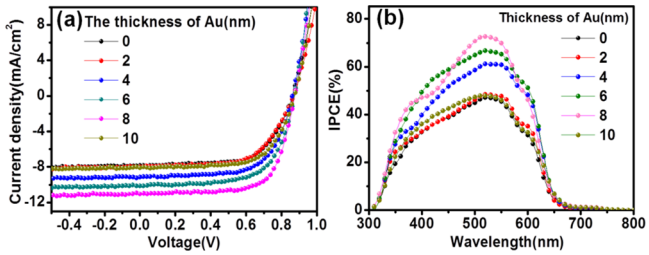

Figure 2. (a) $J-V$ characterization of devices with different thickness of Au NPs tested under AM1.5G solar illuminations. (b) IPCE spectra of devices with different thickness of Au NPs in the wavelength range from 300 to 800 nm.

layer with and without Au NPs, and the corresponding photovoltaic parameters were summarized in Table 1. It is

Table 1. Detail Performance Parameter under 100 mW/cm^2 Simulated AM1.5G in Ambient Air with Different Thickness of Au

thickness of Au (nm)	J_{sc} (mA/cm^2)	V_{oc} (V)	FF (%)	PCE (%)
0	7.87 ± 0.11	0.87 ± 0.01	68.1 ± 0.2	4.67 ± 0.13
2	7.99 ± 0.13	0.87 ± 0.01	68.9 ± 0.2	4.79 ± 0.15
4	9.15 ± 0.14	0.87 ± 0.01	68.4 ± 0.2	5.46 ± 0.15
6	10.13 ± 0.13	0.87 ± 0.01	68.8 ± 0.2	6.01 ± 0.22
8	11.06 ± 0.12	0.87 ± 0.01	68.9 ± 0.2	6.63 ± 0.17
10	8.13 ± 0.15	0.87 ± 0.01	68.2 ± 0.2	4.85 ± 0.18

observed that the device without Au NPs exhibited a relatively low performance, including a short-circuit current (J_{sc}) of 7.87 ± 0.11 mA/cm^2, an open-circuit voltage (V_{oc}) of 0.87 ± 0.01 V, a fill factor (FF) of 68.1 ± 0.2%, and a calculated PCE of 4.67 ± 0.13%. However, the device performance with 8 nm Au contributes a significantly improvement following with a J_{sc} of 11.06 ± 0.12 mA/cm^2, a V_{oc} of 0.87 ± 0.01 V, a FF of 68.9 ±

DOI: 10.1021/acsami.5b05747
ACS Appl. Mater. Interfaces 2015, 7, 18866−18871

0.2% and a PCE of 6.63 ± 0.17%. Observably, the device with x nm-thick Au shows a gradually improved performance, and the optimal thickness is x = 8 nm. It is noted that the device performance is highly sensitive to the amount and diameter of Au NPs embedded into WO_3 buffer layer, and the performance improvement is attributed to SPR of Au NPs. It also can be seen that the value of the V_{oc} for the plasmonic devices with Au NPs have little change compared to the control device without Au NPs, suggesting that the Au NPs have no effect on built-in potential.

To further certify the J_{sc} enhancement, The IPCE of devices with or without Au NPs were measured, and the obtained spectra were plotted in Figure 2b. It is observed that the IPCE variation shows a good agreement with the $J-V$ results. It can be seen that the IPCE of the devices with different thickness of Au shows a significant enhancement in a broad wavelength range of 450−600 nm compared to that of the device without Au NPs, providing a direct evidence for gradually increased J_{sc}. The IPCE results above also clearly indicate that the enhancement in the photovoltaic performance is sensitive to the thickness of Au evaporated into the buffer layers of PSCs. It suggests that the device exhibits the largest improvement due to the strongest SPR effect from 8 nm Au.

The transmittance spectra of devices without top Au electrode were measured to further investigate the mechanism of the J_{sc} improvement, which is shown in Figure 3. As we all

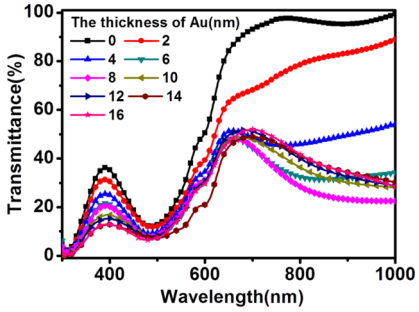

Figure 3. Transmission spectra of devices with different thicknesses of Au NPs without top Au electrode in the wavelength range from 300 to 1000 nm.

know, lower transmittance indicates that more incident light can be trapped within the devices, which can potentially enhance the photon absorption efficiency of the active layer. The result reveals that the absorption is dramatically enhanced from 400 to 600 nm when Au NPs were evaporated inside WO_3 buffer layers. Besides, it is noticed that there is a valley at 500 nm in the transmittance spectra. The valley will lead to a corresponding peak in IPCE, which is in consistent with the observation from IPCE experimental data. Notably, when the wavelength range between 700 to 1000 nm, transmittance curves from the devices with 12−16 nm Au NPs have been almost overlapped. It indicates that when the thickness of Au exceeds 8 nm, the Au films have been formed and can reflect incident light, which results in the uniform transmittance and the disappearance of Au NPs SPR.

The discussion above indicates that the device with 8 nm Au NPs is optimal. To figure out the effect of Au thickness on the film morphology, the AFM images of WO_3 film containing Au NPs (2, 4, 6, 8, 10, 12, 14, 16 nm) were tested in the range of 1 μm and shown in Figure 4a. Moreover, the statistical graph about the relationship between the average size of the Au NPs

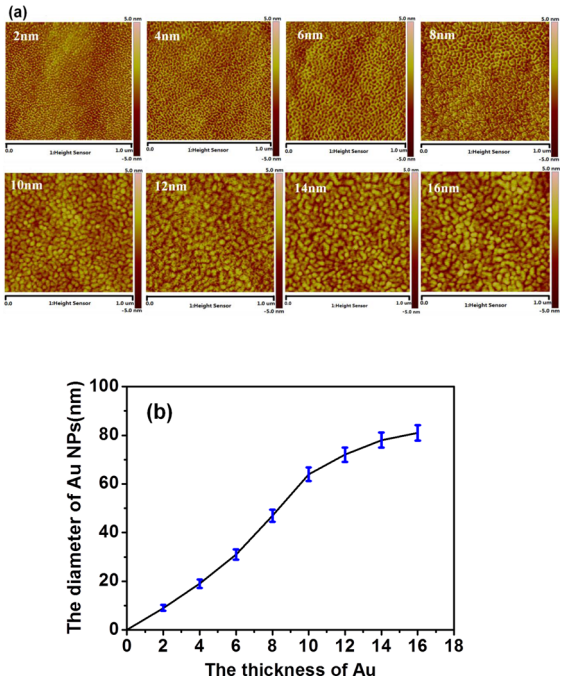

Figure 4. (a) AFM topography images (1 × 1 μm^2) of the WO_3/Au with different thicknesses of Au NPs. (b) The relationship between the average size of the Au NPs and the deposited Au film thickness.

and the deposited film thickness is also shown in Figure 4b. According to previous research, the deposition of Au on thin films will go through four different growth regimes: nucleation, isolated island growth, growth of layer aggregates via partial coalescence, and continuous layer growth.[51,52] It can be clearly seen that Au grows up from nucleation to uniform films with the thickness of Au increases from Figure 4a. The critical thickness of Au film formation was 8 nm because the film morphology is no longer changed when the thickness surpasses 8 nm. It means that the Au metal island acts as Au NPs, which can induce SPR when the thickness of the Au is lower than 8 nm. If the thickness of Au exceeds 8 nm, then the Au films were gradually formed instead of metal island, which results in the case that the Au NP SPR gets weaker or absolutely disappears. The AFM images provide a direct evidence that the device performance variation is dependent on Au NPs diameter, which can induce SPR to enhance light absorption. Notably, the distribution of the Au NPs in the WO_3 layer was uniform, which is attributed to the different surface energy between WO_3 layer and Au. It suggests that the thermally evaporating Au into anode buffer layers is convenient and suitable method to realize the SPR.

The steady state photoluminescence (PL) spectra by using wavelength excitation source (λ_{exc} = 470 nm) are applied to explore the excitons generation behavior of the SPR of devices possessing the structure ITO/TiO_2/P3HT without or with Au NPs, as shown in Figure 5. The absorption in the P3HT was predominately contributed to the exciton generation in the active layer, so we recorded fluorescence spectra of the pristine P3HT. Herein, an obvious enhancement of PL intensity of the sample with 8 nm Au is observed from 650 to 750 nm when excited with 470 nm laser in Figure 5. The remarkable increase in fluorescence intensity results from the increased light absorption in P3HT induced by excitation of the SPR. Hence, the generation rate of excitons was significantly

DOI: 10.1021/acsami.5b05747
ACS Appl. Mater. Interfaces 2015, 7, 18866−18871

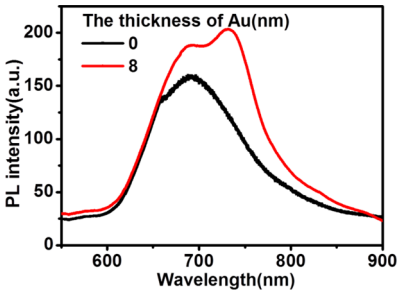

Figure 5. PL spectra of P3HT without or with 8 nm Au NPs tested using an excitation source wavelength (λ_{exc}) of 470 nm.

enhanced due to incorporating Au NPs . A related research was reported by Wu et al. demonstrated that the excitation of the SPR increased the degree of light absorption and enhanced the light excitation rate due to the similar resonance frequency between the Au NPs and the absorption band of P3HT.[53] The enhanced PL provides a direct evidence that Au NPs can effectively improve the light absorption of P3HT.

To further prove the J_{sc} enhancement of devices with Au NPs, the impedance spectroscopy was examined in the dark with an alternating current signal of 1 V in a frequency range of 20 Hz to 2 MHz. The complex impedance spectra of the devices with different thickness of Au are shown in Figure 6a

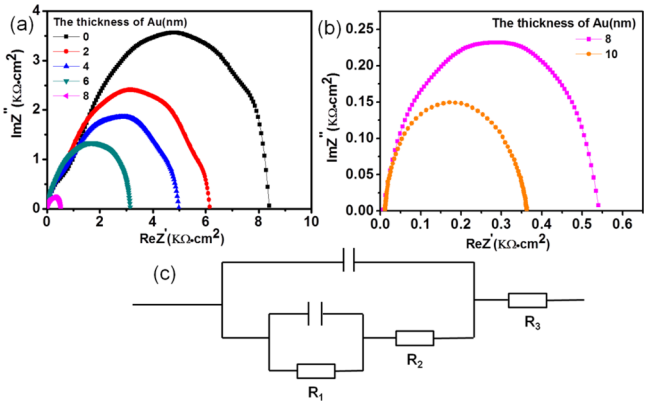

Figure 6. Complex impedance spectra of the devices with different thickness of Au NPs. (a) 0, 2, 4, 6, 8 nm and (b) 8, 10 nm. (c) The fitting model of equivalent circuit.

and b, and the fitting model of equivalent circuit is also given in Figure 6c. Three columns of data were obtained, which are frequency (Hz), impedance, and angle, respectively. The data of *x*-axis are obtained with the formula of impedance × cos(angle/180π), which refers to the real part of the complex impedance, while the data of *y*-axis are obtained with the formula of impedance × sin(angle/180π), which refers to the imaginary part of the complex impedance. As we can see, the shapes of impedance spectra are commendable semicircles that are beneficial to inquiry the resistance in PSCs. In the impedance spectroscopy, the diameters of the semicircles are connected with the device resistance, including recombination resistance (R_1), bulk resistance (R_2), and series resistance (R_3). It can be seen that the diameter of impedance spectroscopy tapers off with the increase of Au thickness. The diameter of device without Au NPs is 2 orders of magnitude larger than that of the devices with 8 nm Au NPs. It indicates that the Au NPs embedded in WO_3 buffer layer can dramatically decrease the device resistance, which is in accordance with J_{sc} variation tendency. Hence, the device with Au NPs can achieve not only higher absorption, but also lower resistance.

3. CONCLUSIONS

In summary, we present a facile thermally evaporated technique to introduce Au NPs into WO_3 buffer layer of inverted PSCs to enhance light absorption by SPR. The AFM images show that a different surface energy between Au and WO_3 leads to Au growing up from nucleation to uniform films. We determined that the PSCs incorporating with 8 nm-thick Au exhibit optimal performance of *J*−*V* and IPCE. The PCE was dramatically improved from 4.67 ± 0.13% to 6.63 ± 0.17% with 8 nm Au NPs. Moreover, the optical absorption enhancement of P3HT layer with 8 nm Au NPs is demonstrated by steady state PL, and the impedance also reveal the device resistance can be decreased with 8 nm Au NPs. The optical and electrical improvement all suggest that thermally evaporating Au into the buffer layer is an appropriate method to further enhance device performance by SPR effect, and the results of this study might pave the way toward higher-efficiency PSCs.

AUTHOR INFORMATION

Corresponding Author

*E-mail: shenliang@jlu.edu.cn (L.S.).

Notes

The authors declare no competing financial interest.

ACKNOWLEDGMENTS

The authors are grateful to National Natural Science Foundation of China (Grant Nos. 61275035, 61370046, 51475200), Key Technology Research and Development Program of Changchun (No.13KG66), and Graduate Innovation Fund of Jilin University (Grant No. 2014021).

REFERENCES

(1) Ng, A.; Yiu, W. K.; Foo, Y.; Shen, Q.; Bejaoui, A.; Zhao, Y.; Gokkaya, H. C.; Djurisic, A. B.; Zapien, J. A.; Chan, W. K.; Surya, C. Enhanced Performance of PTB7:PC(7)(1)BM Solar Cells via Different Morphologies of Gold Nanoparticles. *ACS Appl. Mater. Interfaces* **2014**, *6*, 20676−20684.

(2) Wang, C. C. D.; Choy, W. C. H.; Duan, C.; Fung, D. D. S.; Sha, W. E. I.; Xie, F.-X.; Huang, F.; Cao, Y. Optical and Electrical Effects of Gold Nanoparticles in the Active Layer of Polymer Solar Cells. *J. Mater. Chem.* **2012**, *22*, 1206−1211.

(3) An, C. J.; Yoo, H.-W.; Cho, C.; Park, J.-M.; Choi, J. K.; Jin, M. L.; Lee, J.-Y.; Jung, H.-T. Surface Plasmon Assisted High Performance Top-Illuminated Polymer Solar Cells with Nanostructured Ag Rear Electrodes. *J. Mater. Chem. A* **2014**, *2*, 2915−2921.

(4) Jia, X.; Shen, L.; Yao, M.; Liu, Y.; Yu, W.; Guo, W.; Ruan, S. Highly Efficient Low-Bandgap Polymer Solar Cells with Solution-Processed and Annealing-Free Phosphomolybdic Acid as Hole-Transport Layers. *ACS Appl. Mater. Interfaces* **2015**, *7*, 5367−5372.

(5) Nian, L.; Zhang, W.; Zhu, N.; Liu, L.; Xie, Z.; Wu, H.; Wurthner, F.; Ma, Y. Photoconductive Cathode Interlayer for Highly Efficient Inverted Polymer Solar Cells. *J. Am. Chem. Soc.* **2015**, *137*, 6995−6998.

(6) Kang, H.; Jung, S.; Jeong, S.; Kim, G.; Lee, K. Polymer-Metal Hybrid Transparent Electrodes for Flexible Electronics. *Nat. Commun.* **2015**, *6*, 6503−6510.

(7) Park, B.; Yun, S. H.; Cho, C. Y.; Kim, Y. C.; Shin, J. C.; Jeon, H. G.; Huh, Y. H.; Hwang, I.; Baik, K. Y.; Lee, Y. I.; Uhm, H. S.; Cho, G. S.; Choi, E. H. Surface plasmon excitation in semitransparent inverted polymer photovoltaic devices and their applications as label-free optical sensors. *Light: Sci. Appl.* **2014**, *3*, e222.

DOI: 10.1021/acsami.5b05747
ACS Appl. Mater. Interfaces 2015, 7, 18866−18871

(8) Chen, J.; Cui, C.; Li, Y.; Zhou, L.; Ou, C.; Li, C.; Li, Y.; Tang, J. Single-Junction Polymer Solar Cells Exceeding 10% Power Conversion Efficiency. *Adv. Mater.* **2015**, *27*, 1035−1041.
(9) Vohra, V.; Kawashima, K.; Kakara, T.; Koganezawa, T.; Osaka, I.; Takimiya, K.; Murate, H. Efficient Inverted Polymer Solar Cells Employing Favourable Molecular Orientation. *Nat. Photonics* **2015**, *9*, 403−408.
(10) Chen, C. C.; Chang, W. H.; Yoshimura, K.; Ohya, K.; You, J.; Gao, J.; Hong, Z.; Yang, Y. An Efficient Triple-Junction Polymer Solar Cell Having a Power Conversion Efficiency Exceeding 11%. *Adv. Mater.* **2014**, *26*, 5670−5677.
(11) Li, X.; Xie, F.; Zhang, S.; Hou, J.; Choy, W. MoO_x and V_2O_x as hole and electron transport layers through functionalized intercalation in normal and inverted organic optoelectronic devices. *Light: Sci. Appl.* **2015**, *4*, e273.
(12) Tvingstedt, K.; Persson, N.-K.; Inganäs, O.; Rahachou, A.; Zozoulenko, I. V. Surface Plasmon Increase Absorption in Polymer Photovoltaic Cells. *Appl. Phys. Lett.* **2007**, *91*, 113514.
(13) Beck, F. J.; Polman, A.; Catchpole, K. R. Tunable Light Trapping for Solar Cells Using Localized Surface Plasmons. *J. Appl. Phys.* **2009**, *105*, 114310.
(14) Lin, S.-H.; Lan, S.; Sun, J.-Y.; Lin, C.-F. Influence of Mixed Solvent on the Morphology of the P3HT:Indene-C60 Bisadduct (ICBA) Blend Film and the Performance of Inverted Polymer Solar Cells. *Org. Electron.* **2013**, *14*, 26−31.
(15) Lu, L.; Chen, W.; Xu, T.; Yu, L. High-Performance Ternary Blend Polymer Solar Cells Involving both Energy Transfer and Hole Relay Processes. *Nat. Commun.* **2015**, *6*, 7327−7334.
(16) Park, H.-Y.; Lim, D.; Oh, S.-H.; Kang, P.-H.; Kwak, G.; Jang, S.-Y. Inverted-Structure Polymer Solar Cells Fabricated by Sequential Spraying of Electron-Transport and Photoactive Layers. *Org. Electron.* **2014**, *15*, 2337−2345.
(17) Lu, Z.; Chen, X.; Zhou, J.; Jiang, Z.; Huang, S.; Zhu, F.; Piao, X.; Sun, Z. Performance Enhancement in Inverted Polymer Solar Cells Incorporating Ultrathin Au and LiF Modified ZnO Electron Transporting Interlayer. *Org. Electron.* **2015**, *17*, 364−370.
(18) Kalfagiannis, N.; Karagiannidis, P. G.; Pitsalidis, C.; Panagiotopoulos, N. T.; Gravalidis, C.; Kassavetis, S.; Patsalas, P.; Logothetidis, S. Plasmonic Silver Nanoparticles for Improved Organic Solar Cells. *Sol. Energy Mater. Sol. Cells* **2012**, *104*, 165−174.
(19) Wong, W. Y.; Wang, X. Z.; He, Z.; Djurisic, A. B.; Yip, C. T.; Cheung, K. Y.; Wang, H.; Mak, C. S.; Chan, W. K. Metallated Conjugated Polymers as a New Avenue Towards High-Efficiency Polymer Solar Cells. *Nat. Mater.* **2007**, *6*, 521−527.
(20) Yao, C.; Xu, X.; Wang, J.; Shi, L.; Li, L. Low-Temperature, Solution-Processed Hole Selective Layers for Polymer Solar Cells. *ACS Appl. Mater. Interfaces* **2013**, *5*, 1100−1107.
(21) Zilberberg, K.; Gharbi, H.; Behrendt, A.; Trost, S.; Riedl, T. Low-Temperature, Solution-Processed MoO(x) for Efficient and Stable Organic Solar Cells. *ACS Appl. Mater. Interfaces* **2012**, *4*, 1164−1168.
(22) Long, Y. Improving Optical Performance of Inverted Organic Solar Cells By Microcavity Effect. *Appl. Phys. Lett.* **2009**, *95*, 193301.
(23) Lin, H. W.; Chiu, S. W.; Lin, L. Y.; Hung, Z. Y.; Chen, Y. H.; Lin, F.; Wong, K. T. Device Engineering for Highly Efficient Top-Illuminated Organic Solar Cells with Microcavity Structures. *Adv. Mater.* **2012**, *24*, 2269−2272.
(24) Chen, Y.; Shen, L.; Yu, W.; Long, Y.; Guo, W.; Chen, W.; Ruan, S. Highly Efficient ITO-Free Polymer Solar Cells Based on Metal Resonant Microcavity Using WO_3/Au/WO_3 as Transparent Electrodes. *Org. Electron.* **2014**, *15*, 1545−1551.
(25) Yu, W.; Shen, L.; Meng, F.; Long, Y.; Ruan, S.; Chen, W. Effects of the Optical Microcavity on the Performance of ITO-Free Polymer Solar Cells with WO_3/Ag/WO_3 Transparent Electrode. *Sol. Energy Mater. Sol. Cells* **2012**, *100*, 226−230.
(26) Lai, Y.-Y.; Lan, Y.-P.; Lu, T.-C. Strong light−matter interaction in ZnO microcavities. *Light: Sci. Appl.* **2013**, *2*, e76.
(27) Yu, W.; Shen, L.; Long, Y.; Shen, P.; Guo, W.; Chen, W.; Ruan, S. Highly Efficient and High Transmittance Semitransparent Polymer Solar Cells with One-Dimensional Photonic Crystals as Distributed Bragg Reflectors. *Org. Electron.* **2014**, *15*, 470−477.
(28) Zhou, D.; Biswas, R. Photonic Crystal Enhanced Light-Trapping in Thin Film Solar Cells. *J. Appl. Phys.* **2008**, *103*, 093102−093108.
(29) Shi, X.; Shi, L.; Li, M.; Hou, J.; Chen, L.; Ye, C.; Shen, W.; Jiang, L.; Song, Y. Efficient Luminescence of Long Persistent Phosphor Combined with Photonic Crystal. *ACS Appl. Mater. Interfaces* **2014**, *6*, 6317−6321.
(30) Yu, W.; Shen, L.; Shen, P.; Long, Y.; Sun, H.; Chen, W.; Ruan, S. Semitransparent Polymer Solar Cells with 5% Power Conversion Efficiency Using Photonic Crystal Reflector. *ACS Appl. Mater. Interfaces* **2014**, *6*, 599−605.
(31) Su, Y. H.; Ke, Y.-F.; Cai, S.-L.; Yao, Q.-Y. Surface plasmon resonance of layer-by-layer gold nanoparticles induced photoelectric current in environmentally-friendly plasmon-sensitized solar cell. *Light: Sci. Appl.* **2012**, *1*, e14.
(32) Jägeler-Hoheisel, T.; Selzer, F.; Riede, M.; Leo, K. Direct Electrical Evidence of Plasmonic Near-Field Enhancement in Small Molecule Organic Solar Cells. *J. Phys. Chem. C* **2014**, *118*, 15128−15135.
(33) Lepage, D.; Jiménez, A.; Beauvais, J.; Dubowski, J. Conic hyperspectral dispersion mapping applied to semiconductor plasmonics. *Light: Sci. Appl.* **2012**, *1*, e28.
(34) Rand, B. P.; Peumans, P.; Forrest, S. R. Long-Range Absorption Enhancement in Organic Tandem Thin-Film Solar Cells Containing Silver Nanoclusters. *J. Appl. Phys.* **2004**, *96*, 7519−7528.
(35) Chen, X.; Jia, B.; Zhang, Y.; Gu, M. Exceeding the limit of plasmonic light trapping in textured screen-printed solar cells using Al nanoparticles and wrinkle-like graphene sheets. *Light: Sci. Appl.* **2013**, *2*, e92.
(36) Hägglund, C.; Zäch, M.; Kasemo, B. Enhanced Charge Carrier Generation in Dye Sensitized Solar Cells by Nanoparticle Plasmons. *Appl. Phys. Lett.* **2008**, *92*, 013113.
(37) Cole, J. R.; Halas, N. J. Optimized Plasmonic Nanoparticle Distributions for Solar Spectrum Harvesting. *Appl. Phys. Lett.* **2006**, *89*, 153120.
(38) Guo, C.; Sun, T.; Cao, F.; Liu, Q.; Ren, Z. Metallic nanostructures for light trapping in energy-harvesting devices. *Light: Sci. Appl.* **2014**, *3*, e161.
(39) Chuang, M. K.; Chen, F. C. Synergistic Plasmonic Effects of Metal Nanoparticle-Decorated PEGylated Graphene Oxides in Polymer Solar Cells. *ACS Appl. Mater. Interfaces* **2015**, *7*, 7397−7405.
(40) Fan, X.; Zheng, W.; Singh, D. Light scattering and surface plasmons on small spherical particles. *Light: Sci. Appl.* **2014**, *3*, e179.
(41) Lu, L.; Luo, Z.; Xu, T.; Yu, L. Cooperative Plasmonic Effect of Ag and Au Nanoparticles on Enhancing Performance of Polymer Solar Cells. *Nano Lett.* **2013**, *13*, 59−64.
(42) Pors, A.; Nielsen, M. G.; Bernardin, T.; Weeber, J.-C.; Bozhevolnyi, S. I. Efficient unidirectional polarization-controlled excitation of surface plasmon polaritons. *Light: Sci. Appl.* **2014**, *3*, e197.
(43) Chen, X.; Zhao, C.; Rothberg, L.; Ng, M.-K. Plasmon Enhancement of Bulk Heterojunction Organic Photovoltaic Devices by Electrode Modification. *Appl. Phys. Lett.* **2008**, *93*, 123302.
(44) Zijlstra, P.; Chon, J. W.; Gu, M. Five-Dimensional Optical Recording Mediated by Surface Plasmons in Gold Nanorods. *Nature* **2009**, *459*, 410−413.
(45) Hsiao, Y.-S.; Charan, S.; Wu, F.-Y.; Chien, F.-C.; Chu, C.-W.; Chen, P.; Chen, F.-C. Improving the Light Trapping Efficiency of Plasmonic Polymer Solar Cells through Photon Management. *J. Phys. Chem. C* **2012**, *116*, 20731−20737.
(46) Su, Z.; Wang, L.; Li, Y.; Zhang, G.; Zhao, H.; Yang, H.; Ma, Y.; Chu, B.; Li, W. Surface Plasmon Enhanced Organic Solar Cells with a MoO_3 Buffer Layer. *ACS Appl. Mater. Interfaces* **2013**, *5*, 12847−12853.
(47) You, J.; Chen, C. C.; Dou, L.; Murase, S.; Duan, H. S.; Hawks, S. A.; Xu, T.; Son, H. J.; Yu, L.; Li, G.; Yang, Y. Metal Oxide Nanoparticles as an Electron-Transport Layer in High-Performance and Stable Inverted Polymer Solar Cells. *Adv. Mater.* **2012**, *24*, 5267−5272.

DOI: 10.1021/acsami.5b05747
ACS Appl. Mater. Interfaces 2015, 7, 18866−18871

(48) Li, H.; Cao, J.; Zhou, Q.; Ding, L.; Wang, J. High-Performance Inverted PThTPTI:$PC_{71}BM$ Solar Cells. *Nano Energy* **2015**, *15*, 125−134.
(49) Xu, P.; Shen, L.; Meng, F.; Zhang, J.; Xie, W.; Yu, W.; Guo, W.; Jia, X.; Ruan, S. The Role of Ag Nanoparticles in Inverted Polymer Solar Cells: Surface Plasmon Resonance and Backscattering Centers. *Appl. Phys. Lett.* **2013**, *102*, 123301.
(50) Tao, C.; Ruan, S.; Xie, G.; Kong, X.; Shen, L.; Meng, F.; Liu, C.; Zhang, X.; Dong, W.; Chen, W. Role of tungsten oxide in inverted polymer solar cells. *Appl. Phys. Lett.* **2009**, *94*, 043311.
(51) Schwartzkopf, M.; Santoro, G.; Brett, C. J.; Rothkirch, A.; Polonskyi, O.; Hinz, A.; Metwalli, E.; Yao, Y.; Strunskus, T.; Faupel, F.; Muller-Buschbaum, P.; Roth, S. V. Real-Time Monitoring of Morphology and Optical Properties during Sputter Deposition for Tailoring Metal-Polymer Interfaces. *ACS Appl. Mater. Interfaces* **2015**, *7*, 13547−13556.
(52) Schwartzkopf, M.; Buffet, A.; Korstgens, V.; Metwalli, E.; Schlage, K.; Benecke, G.; Perlich, J.; Rawolle, M.; Rothkirch, A.; Heidmann, B.; Herzog, G.; Muller-Buschbaum, P.; Rohlsberger, R.; Gehrke, R.; Stribeck, N.; Roth, S. V. From Atoms to Layers: in Situ Gold Cluster Growth Kinetics during Sputter Deposition. *Nanoscale* **2013**, *5*, 5053−5062.
(53) Wu, J.-H.; Chen, F.-C.; Hsiao, Y.-S.; Chien, F.-C.; Chen, P.; Kuo, C.-H.; Huang, M., H.; Hsu, C.-S. Surface Plasmonic Effects of Metallic Nanoparticles on the Performance of Polymer Bulk Heterojunction Solar Cells. *ACS Nano* **2011**, *5*, 959−967.

DOI: 10.1021/acsami.5b05747
ACS Appl. Mater. Interfaces 2015, 7, 18866−18871